



# A priori analysis of the performance of cross hot-wire probes in a rough wall boundary layer based on stereoscopic PIV

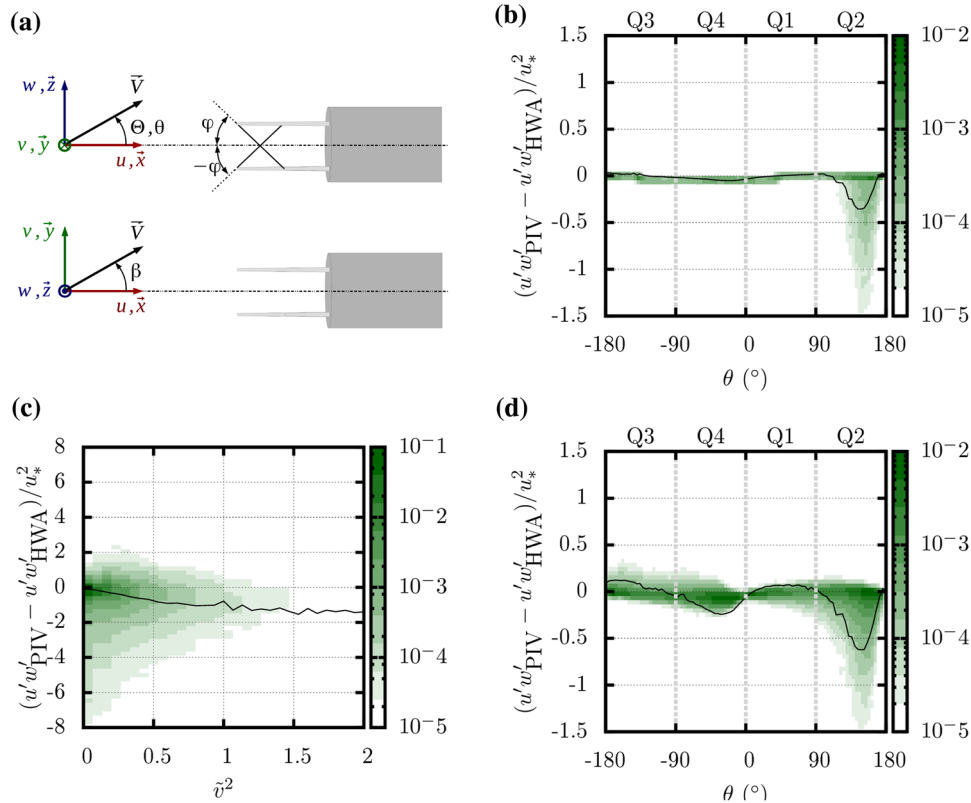
Laurent Perret<sup>1</sup> · Cédric Rivet<sup>1</sup>

Received: 15 June 2018 / Revised: 6 August 2018 / Accepted: 11 September 2018 / Published online: 21 September 2018  
© Springer-Verlag GmbH Germany, part of Springer Nature 2018

## Abstract

Error in measuring Reynolds shear-stress in turbulent boundary layer flows over a rough surface with a cross hot-wire has been reported in the literature and attributed to the existence of strong ejection and sweep motions that cause rectification, e.g. deviation of the velocity vector angle outside the acceptance cone of these probes. Using stereoscopic particle image velocimetry measurements and the concept of effective cooling velocities, the objective of the present study is to perform an a priori analysis of the cause of errors occurring when employing cross hot-wire anemometers. Besides the above-mentioned rectification effect, the role of the non-measured component is investigated. It is shown to be responsible for a non-negligible underestimation of the measured velocity variances and Reynolds shear-stress. This often overlooked source of error is intrinsic to turbulent flows and not limited to flow over rough walls.

**Graphical abstract** Error analysis on the instantaneous shear-stress in the roughness sublayer of a rough boundary-layer measured by a (a) generic XHWA modeled using SPIV data : (c) influence of the non-measured component  $v$ , and relationships with Q-events (b) without and (d) with the non-measured component influence.



### 1 Introduction

Despite the availability of laser doppler velocimetry (LDV) or particle image velocimetry (PIV), hot-wire anemometry (HWA) is still widely used in research laboratories for the study of turbulent flows. This measurement method is indeed still one of the easiest to set up and use, it does not present the safety problems that LDV or PIV show due the use of high-energy laser or the necessity of seeding the flow, and it allows for evenly sampled turbulence measurements with unsurpassed acquisition rates. Combination of several hot-wires can give access to several velocity components. In particular, cross hot-wire anemometry (XHWA hereafter) is one of the most widely employed probe configuration as it allows for the estimation of the Reynolds shear-stress  $\langle u'w' \rangle$  (where  $\langle \rangle$  represents classical ensemble averaging,  $u$  and  $w$  are the velocity components along the streamwise and wall-normal directions, respectively, and  $u'$  denotes the fluctuating part of  $u$  over its mean  $\langle u \rangle$ ), a quantity usually used to estimate the friction velocity  $u_*$  in boundary layers developing over rough walls. Indeed, given the complex geometry of the wall, and in the absence of direct means of drag measurement such as a drag balance, one has to resort to the measurement of

the Reynolds shear-stress to obtain an indirect estimation of the friction velocity as  $u_* = (-\langle u'w' \rangle)^{1/2}$  (Cheng and Castro 2002). Accurate measurements of the evolution with wall-normal distance of the variance of both the wall-normal velocity component and the Reynolds shear-stress are also of crucial importance to assess the influence of the wall roughness on the structure of boundary layer flows (Djenidi et al. 2014). Despite its obvious advantages, XHWA is affected by several sources of error in high turbulence intensity flows such as the rectification effect (i.e. the fact that the instantaneous angle of the velocity vector can go beyond the acceptance cone of the probe), the influence of the non-measured velocity component (i.e. the component normal to the wire plane, denoted  $v$  in the present case), the spatial resolution or the effect of the finite separation between the wires (Müller 1992; Tagawa et al. 1992; Tutu and Chevray 1975). These shortcomings can lead to a non-negligible underestimation of  $\langle u'w' \rangle$ , a bias consistently reported in studies of boundary layer flows developing over large roughness elements, and which has been attributed to the highly turbulent nature of the flow and the existence of intense ejection and penetration events (Djenidi et al. 2014; Reynolds and Castro 2008). As noted by Djenidi et al. (2014) in their recent investigation

(based on two-component PIV measurements) of the possible source of errors in XHWA data obtained in flows over 2D rough wall, the uncertainty of XHWA performance has lead to some “controversy” about the structure of boundary layer flows over rough wall, namely how roughness can affect the outer layer of the flow, depending on its geometry (i.e. 2D or 3D roughness elements). As recalled by Djenidi et al. (2014) and Antonia and Djenidi (2010) suggested that DNS database should be used to investigate XHWA shortcomings such as the effect of wire length or the separation between wires. However, this type of analysis may suffer from low Reynolds number effect and limited ratio between the depth of the boundary layer and the height of the roughness elements.

Building upon the recent results of Djenidi et al. (2014), the objective of the present study is to investigate the possible influence of the non-measured velocity component, normal to the plane formed by the two wires. The present work considers a modeled generic XHWA probe that would be employed to measure the streamwise and wall-normal velocity components  $u$  and  $w$  parallel to the wire plane. The flow configuration corresponds to a high-Reynolds number boundary layer ( $\delta u_* / \nu = 32,400$ ) developing over a staggered cube array representative of the lower part of the atmospheric boundary layer developing over a suburban terrain (Blackman et al. 2017; Perret et al. 2018; Rivet 2014). Instantaneous three-component stereoscopic PIV (SPIV) measurements performed in a wall-normal plane are used to feed the equations for the effective cooling velocities  $U_{\text{eff}}$  of the two wires proposed by Tutu and Chevray (1975) which

include as parameters the angle formed by the two wires with the probe axis and the sensitivity coefficients of the wires to the normal and the tangential velocity components. Using this three-component velocity dataset and the XHWA probe model allows us to literally turn on and off the non-measured velocity component and analyse the impact of its presence on the XHWA probe performance.

The following section provides a short description of the experimental setup and the presentation of the methodology employed to conduct the proposed analysis. Section 3 presents the main flow characteristics and the obtained results. Conclusions are provided in the last section.

## 2 Experimental setup and methods

In the following,  $x$ ,  $y$  and  $z$  denote the streamwise, spanwise and wall-normal directions, respectively (Fig. 1), and  $u$ ,  $v$ , and  $w$  the streamwise, spanwise, and wall-normal velocity components, respectively. The superscript “+” denotes quantities normalized with inner scales, namely the friction velocity  $u_*$  and the kinematic viscosity  $\nu$ .

### 2.1 Experimental setup

Only the main characteristics of the experimental setup are provided here, the reader being referred to the work of Rivet (2014) for an extensive description of the wind tunnel and the PIV setup. The flow characteristics are presented in Sect. 3.1 and Table 1. Experiments were performed in

**Fig. 1** Schematic representation of **a** the atmospheric the wind tunnel, **b** the stereoscopic PIV setup and **c** the generic XHWA probe (top: side view, bottom: top view)

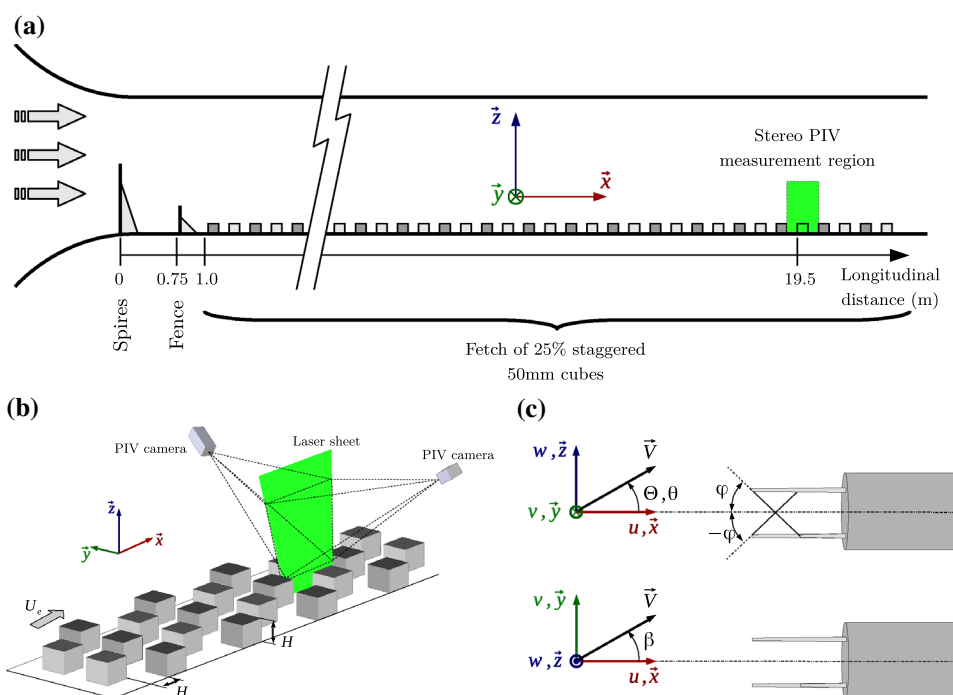


**Table 1** Characteristics of the boundary layer where  $\lambda_p$  is the plan area density,  $U_e$  the freestream velocity,  $d$  the displacement height,  $z_0$  the roughness length and  $z_{\text{RSL}}$  the upper limit of the roughness sublayer (Rivet 2014)

$\lambda_p$ (%)	$U_e$ (m/s)	$u_*/U_e$	$\delta/H$	$H^+$	$\delta^+$	$d/H$	$z_0/H$	$z_{\text{RSL}}/H$
25	5.77	0.073	22.7	1430	32,400	0.59	0.11	2.0

the boundary layer wind tunnel at LHEEA, Nantes, France which has a 24 m  $\times$  2 m  $\times$  2 m working section (Fig. 1a). The simulation at the scale 1:200 of a suburban-type atmospheric boundary layer developing over an idealized canopy model was achieved using five vertical, tapered spires of height of 800 mm and width of 134 mm at their base, a 200-mm high solid fence across the working section located 0.75 m downstream of the inlet, followed by a 22-m fetch of staggered cube roughness elements with a plan area density of  $\lambda_p = 25\%$ . The cube height was  $H = 50$  mm. The measurements were performed with a free stream velocity  $5.77 \text{ m s}^{-1}$ , at a longitudinal location of 19.5 m after the end of the contraction. Stereoscopic PIV measurements were conducted in a wall-normal plane aligned with the main flow, in the center of the test section. Two 2048  $\times$  2048 pixels 12 bits camera equipped with 105-mm objective lenses were employed in a stereoscopic configuration satisfying the Scheimpflug condition (Fig. 1b). A Litron 200-mJ Nd-YAG laser, located under the wind tunnel floor, was employed to illuminate the region of interest. The time delay between two consecutive images for PIV processing was set to  $dt = 500 \mu\text{s}$ . The flow was seeded with glycol/water droplets (typical size  $1 \mu\text{m}$ ) using a fog generator. Both the synchronization between the laser and the cameras, and the calculation of the PIV velocity vector fields were performed using the Dantec FlowDynamics software. A set of  $N = 4000$  velocity fields was recorded. A FFT-based 2D-PIV algorithm with sub-pixel refinement was employed with  $32 \times 32$  final interrogation windows, using an overlap of 50%. Spurious vectors were detected by an automatic validation procedure whereby the SNR of the correlation peak had to exceed a minimum value, and the vector amplitude had to be within a certain range of the local median to be considered as valid. Once spurious vectors had been detected, they were replaced by vectors resulting from a linear interpolation in each direction from the surrounding  $3 \times 3$  set of vectors. A pinhole model was employed to reconstruct the three-component vector fields from the two-component vector fields from each camera. The final spatial resolution is  $\Delta_x/H = 0.034$  ( $\Delta_x^+ = 48$  or  $\Delta_x = 1.7$  mm) and  $\Delta_z/H = 0.044$  ( $\Delta_z^+ = 61$  or  $\Delta_z = 2.2$  mm) in the streamwise and wall-normal directions, respectively. In their study of the turbulent kinetic energy budget in the same flow configuration, using the exact same experimental setup as in the present study, Blackman et al. (2017) have estimated  $\lambda$  the Taylor microscale and  $\eta$  the Kolmogorov scale to be in the range  $0.12 < \lambda/H < 0.29$  and  $0.004 < \eta/H < 0.006$ ,

respectively, for  $0 < z/H < 5$ . Therefore, while the spatial resolution of the present PIV measurements is too large to capture the smallest velocity scales in the dissipative range that are filtered out or attenuated, scales in the inertial range are expected to be correctly measured. It must be noted here that the spatial resolution of the present PIV measurements is in the same range as the wire-length of commercially available HWA probes commonly used for the investigation of turbulent flows (1.25 mm for Dantec Dynamics 55P11 single probes and 55P61 XHWA for instance). The influence of the spatial filtering of the smallest scales on the estimation of large instantaneous flow angle events is further analysed in Sect. 3.1 via comparison with the results from the DNS of Coceal et al. (2007).

## 2.2 Modeling the cross hot-wire probe

As introduced by Tutu and Chevray (1975) and later used by Tagawa et al. (1992), the present study relies on the modeling of a generic cross hot-wire probes using the concept of effective cooling velocities which links the three velocity components of the investigated flow to the instantaneous cooling velocity that controls the thermal exchange between each wire of the probe and the fluid. A schematic representation of such a probe is provided in Fig. 1c, in which  $\theta$  is the instantaneous angle between the longitudinal probe axis and the velocity vector in the  $x - z$  plane defined using  $u$  and  $w$ ,  $\theta$  the angle based on the fluctuating velocity components  $u'$  and  $w'$  (i.e.  $\theta = \arg(u' + iw')$ , with  $i^2 = -1$ ) and  $\beta$  the angle defined in the  $x - y$  plane based on the fluctuating velocity components  $u'$  and  $v'$  (i.e.  $\beta = \arg(u' + iv')$ ). Only probes symmetric with respect to their longitudinal axis are considered here.

When the XHWA probe is set to measure  $u$  and  $w$ , each wire being sensitive (but differently) to both the normal and tangential velocity components, the effective cooling velocities read:

$$\begin{cases} U_{\text{eff1}}^2 = u^2 + h^2v^2 + w^2 - (1 - k^2)[u \cos(\phi) - w \sin(\phi)]^2 \\ U_{\text{eff2}}^2 = u^2 + h^2v^2 + w^2 - (1 - k^2)[u \cos(-\phi) - w \sin(-\phi)]^2, \end{cases} \quad (1)$$

where  $U_{\text{eff1}}$  and  $U_{\text{eff2}}$  are the cooling velocities of the wires at an angle  $\phi$  and  $-\phi$  with the mean streamwise velocity component  $\langle u \rangle$ , respectively, and  $h$  and  $k$  are sensitivity coefficients of the wires to the normal and the tangential velocity components, respectively. These two effective cooling

velocities can be recombined to compute the velocity components  $u_{\text{HWA}}$  and  $w_{\text{HWA}}$  measured by the virtual XHWA probe. This recombination corresponds to the probe calibration that is usually performed in laminar or low-turbulence level flow by varying the wind speed and rotating the probe around an axis normal to the  $u - w$  plane. This commonly used calibration process does not take into account the effect of the non-measured velocity component  $v$ , i.e.  $u_{\text{HWA}}$  and  $w_{\text{HWA}} = f(U_{\text{eff1}}^2, U_{\text{eff2}}^2, k, \phi)$ . Solving Eq. (1) for  $u_{\text{HWA}}$  and  $w_{\text{HWA}}$  as a function of  $U_{\text{eff1}}$  and  $U_{\text{eff2}}$  is, therefore, achieved by dropping the terms involving  $v$  so that only two unknowns  $u$  and  $w$  are left in the set of two equations (see Tagawa et al. 1992 for more details). In the present study, the SPIV data are used as inputs to obtain simulated  $u_{\text{HWA}}$  and  $w_{\text{HWA}}$  velocity components as measured by a virtual XHWA probe subjected to the investigated three-component flow field: for each SPIV field, at each location  $x, z$ , the velocity components  $u_{\text{PIV}}, v_{\text{PIV}}$  and  $w_{\text{PIV}}$ , are used in Eq. (1) to compute  $U_{\text{eff1}}$  and  $U_{\text{eff2}}$  which are then recombined to estimate  $u_{\text{HWA}}$  and  $w_{\text{HWA}}$  using the approach from Tagawa et al. (1992). The simulated effective cooling velocities are, therefore, the results of the complete interaction of the flow with both wires and account for the probe geometry. The sensitivity coefficients  $h$  and  $k$  can be set to zero independently to investigate the influence of the  $v$  component (via  $h$ ) and the influence of the velocity component tangential to each wire (via  $k$ ). If non-zero,  $h$  and  $k$  are set to 1.05 and 0.2, respectively, values usually reported in the literature (Bruun 1995; Tagawa et al. 1992; Tutu and Chevray 1975). Contrary to Tagawa et al. (1992), the effect of wire separation that can lead to a certain degree of decorrelation of the velocities sensed by the wires is not accounted for in the present study. Finally, it is worth mentioning that the same approach can be employed to model a single-wire probe using only one of the two equations in Eq. (1). While it is beyond the scope of the present paper, a brief comparison of the performance of XHWA and single-wire probes is presented in Sect. 3.2 for the sake of completeness.

### 3 Results

In the following, the Reynolds decomposition is used to decompose any quantity  $u$  into its fluctuating part  $u'$  and its mean  $\langle u \rangle$ , where  $\langle \rangle$  represents the ensemble average over both time and the streamwise direction  $x$ . The standard deviation of  $u$  is denoted  $\sigma_u = \langle u'^2 \rangle^{1/2}$ . Because the focus of the present study is on the probe performance rather than the detailed characteristics of the flow, spatial averaging along the streamwise direction is employed here as a way to improve the statistical significance of the estimated probability density functions even if the flow is non-homogeneous in this direction in the region close to the roughness elements.

Subscripts PIV and HWA denote the velocity field originally measured via SPIV and obtained from the XHWA probe model, respectively.

#### 3.1 Boundary layer characteristics

In the following, the wall-normal evolution of the mean streamwise velocity component is described via its meteorological form, namely  $\langle u \rangle = u_* / \kappa \ln[(z - d)/z_0]$ , where  $\kappa = 0.4$  is the Von Karman constant. The main flow characteristics reported in Table 1 show that the simulation of a high-Reynolds number atmospheric boundary layer is achieved ( $\delta^+ = \delta u_* / \nu = 32,400$ ), whose displacement height  $d$  and roughness height  $z_0$  are those of an urban boundary layer. The value of  $u_*$  reported in Table 1 has been obtained via the form drag measurement of a roughness element using a cube instrumented for wall-pressure measurement as in Cheng and Castro (2002) and (Perret et al. 2017, 2018). The reader is referred to the work of Basley et al. (2018), Perret et al. (2017, 2018) and Rivet (2014) for more details regarding the scaling of the flow and its statistics. In these studies, different methods have been used to estimate the friction velocity  $u_*$  (either from the Reynolds shear-stress wall-normal profile or from form drag measurements), leading to slightly different values which has no consequence on the present results and conclusions.

Profiles throughout the entire boundary layer of both the mean and the variance of the streamwise velocity component are shown in Fig. 2a, confirming the presence of a well-developed logarithmic region. Comparison with the HWA profiles of Perret et al. (2017, 2018) and the LDV measurements of Herpin et al. (2018) performed in the same flow configuration at a few wall-normal locations, 1  $H$  downstream of a cube, demonstrates the absence of bias in the present PIV measurements. The underestimation of the variance by the present PIV data at the lowest wall-normal locations is attributed to the fact that the present data have been spatially averaged along the streamwise direction  $x$  while HWA and LDV data have been acquired at one single location (1  $H$  downstream of a cube). Comparison of the local flow statistics measured at  $x = H/2$  downstream of a cube, on the cube centerline [point referred to as P1 in Castro et al. (2006)] as a function of  $(z - d)/\delta$  to account for Reynolds number difference, are compared to LDV measurements from Castro et al. (2006) in Fig. 2b. Given the scatter of the LDV data and the difference of Reynolds number ( $\delta^+ = 32,400$  vs 6900), a rather good agreement is obtained in most of the measurement region. The present results show a global underestimation of the standard deviation of the lateral velocity component  $v$  and of both that of  $w$  and the Reynolds shear-stress in the region very close to the canopy. It must be noted that the point P1 at which the comparison is performed is located close to a cube, where

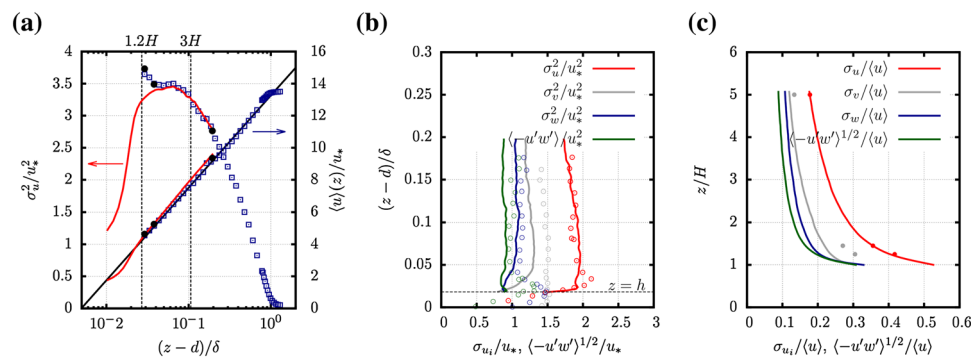


**Fig. 2** **a** Wall-normal evolution of the mean streamwise velocity component  $\langle u \rangle$  and the variance  $\sigma_u^2$  normalized by  $u_*$  obtained (red open circles) via SPIV (present data) and (blue open squares) HWA from Perret et al. (2018). Black filled circles show results from the LDV measurements of Herpin et al. (2018) in the same flow configuration. The solid black line shows the theoretical logarithmic law. The vertical dashed lines show the locations where detailed error analysis is performed (see text). **b** Wall-normal evolution of the local standard deviation of the three velocity components and the Reynolds shear-

stress normalized by the friction velocity  $u_*$  measured at  $x = H/2$  downstream of a cube, on the cube centerline (point P1). Lines: present data, open circles: LDV data from Castro et al. (2006). **c** Wall-normal evolution of the standard deviation of the three velocity components and Reynolds shear-stress normalized by the local mean streamwise velocity  $\langle u \rangle$  (SPIV measurements). Symbols show results for (red) the streamwise and (gray) the spanwise velocity components from the LDV measurements of Herpin et al. (2018) in the same flow configuration

the aforementioned lower spatial resolution of the present PIV measurement is maybe more critical than elsewhere. As demonstrated below, these discrepancies are unlikely to affect the conclusion of the present analysis regarding the XHWA performance as the present PIV measurements are shown to be able to capture the global flow structure in terms of frequency and shear-stress contribution of velocity fluctuations. Figure 2c shows profiles of the turbulence intensities of the three velocity components and the normalized Reynolds shear-stress  $\langle u'w' \rangle$  measured in the lowest part of the boundary layer via SPIV. Comparison with the LDV measurements of Herpin et al. (2018) confirms the correct estimation the streamwise velocity component but also the underestimation of the turbulent intensity of the spanwise velocity component  $v$  in the present PIV data. This bias is attributed to the fact that  $v$ , being the out-of-plane velocity component, is influenced by the already mentioned spatial filtering of the PIV technique of both components  $u$  and  $w$ . In the investigated region, turbulence intensities are always higher than 10%, reaching 50% at canopy top for the streamwise velocity component, confirming that this region, of crucial interest for the study of the roughness sublayer and the constant shear-stress region (Rivet 2014), is particularly challenging for thermal anemometry. It must be noted here that the turbulence intensity of the lateral velocity component  $v$ , rarely reported in the literature, is larger than that of  $w$ , in most of the investigated region.

To further confirm the adequacy of the present PIV measurements to assess the XHWA performance, a quadrant analysis is performed to analyse the frequency of occurrence and contribution to Reynolds shear-stress  $\langle u'w' \rangle$  of velocity fluctuations when partitioning the flow into Q1 ( $u' > 0$  and

$w' > 0$ ), Q2 ( $u' < 0$  and  $w' > 0$ ), Q3 ( $u' < 0$  and  $w' < 0$ ) and Q4 ( $u' > 0$  and  $w' < 0$ ) events. Results are analysed in terms of the relative number of each type of event, the relative magnitude of their contribution to  $\langle u'w' \rangle$ , defined as a fraction of the sum of the magnitudes in all the quadrants and the relative number of ejections and sweeps, and their relative contribution to the Reynolds stress. As in Coceal et al. (2007) who performed a DNS of the turbulent flow developing over a staggered cube array with the same plan density (25%) as in the present work, wall-normal evolution of spatially averaged statistics is considered (Fig. 3). Present results confirm that Q2 and Q4 are the most numerous events and the major contributors to the total shear-stress. Close to the canopy top, predominance, in terms of frequency, of ejection (Q2) over sweep (Q4) events is also demonstrated, while it is the opposite in terms of contribution to the shear-stress, in agreement with the literature (Castro et al. 2006; Coceal et al. 2007). Finally, a good agreement between the present results and those from Coceal et al. (2007) is shown, for all the analysed quantities, demonstrating that the present measurement setup correctly captures the structure of the investigated turbulent flow.

Based on the comparison of the present flow statistics with those available from the literature in similar flow configurations, the present measurements have been shown to be able to capture all the salient features of turbulent flows developing over large roughness elements as well as the coherent structures contributing to the Reynolds shear-stress. Given the high level of fluctuation of the lateral velocity component  $v$ , a bias of the velocity components  $u_{\text{HWA}}$  and  $w_{\text{HWA}}$  measured by XHWA can be anticipated. However, it must be noted here that given the apparent underestimation

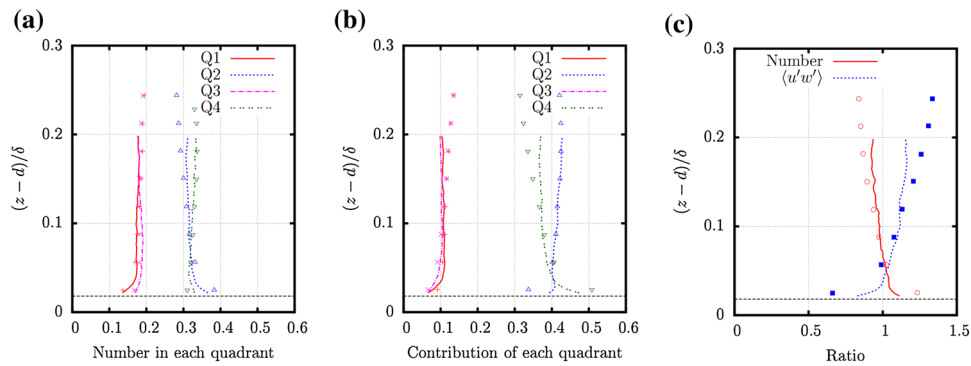


**Fig. 3** Wall-normal evolution of **a** the relative number of events in each quadrant, **b** the relative contribution to  $u'w'$  of events in each quadrant. Red plus signs and solid line: Q1, blue triangles up and dashed line: Q2, magenta crosses and dashed-dotted line: Q3, green triangles down and double dotted lines: Q4. **c** Ratio of number (red

solid line and circles) and contribution to  $\langle u'w' \rangle$  (blue dashed line and squares) of Q2 events to that of Q4 events. Lines show the present results while symbols are for the results of the DNS of Coceal et al. (2007)

of  $\sigma_v$  compared to that reported in the literature, the influence of  $v$  on the XHWA probe performance is likely to be underestimated in the present analysis.

### 3.2 XHWA error

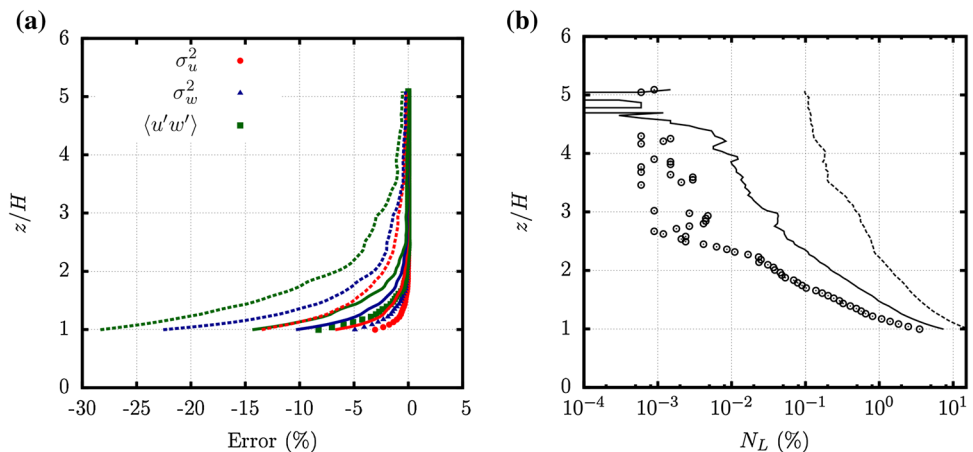
The methodology presented in Sect. 2.2 is employed here to simulate XHWA measurements in the region corresponding to  $1 < z/H < 5$ . The effect of the wire cooling by the tangential velocity is not considered here ( $k = 0$ ) as it has been well studied in the past (Tutu and Chevray 1975).

The focus is first on the rectification effect that is the influence of the wire angle  $\phi$  and its link with the angle  $\Theta$  between the instantaneous velocity vector and the direction of the mean flow. It is shown in Fig. 4a that, as expected, the relative error  $(\sigma_{u_{XHWA}}^2 - \sigma_{u_{PIV}}^2) / \sigma_{u_{PIV}}^2$  between the original statistics from the SPIV and those calculated from the simulated XHWA signals increases with decreasing wire angle. This error increase is directly linked to a reduction of the

acceptance cone angle of the probe when  $\phi$  decreases, the instantaneous flow angle  $\Theta$  lying more frequently outside the acceptable angle range (taken here as  $\pm\phi$ ) as shown by the evolution of the frequency  $N_L$  of having  $|\Theta| > \phi$  in Fig. 4b.

The influence of the non-measured velocity component  $v$  (which is normal to the plane  $x - z$  formed by the two wires) is investigated by setting  $h$  to 0 or 1.05 while keeping  $\phi = 45^\circ$  and  $k = 0$ . The relative error between the original SPIV statistics and those estimated from the XHWA probe is shown in Fig. 5. Taking into account, the lateral velocity component ( $h = 1.05$ ) has a dramatic effect on the statistics of the measured velocity components, the relative error increasing by a factor of two when compared to the case where this bias is not accounted for ( $h = 0$ ). As with the effect of the wire angle, the bias is towards a systematic underestimation by the XHWA of all the statistics, the Reynolds shear-stress and the variance of the wall-normal velocity component  $w$  being the most affected. Error in the variance of  $u$  is indeed below 3% in the region  $z/H > 2$ , where rectification effects are negligible. This is in full agreement

**Fig. 4** Wall-normal evolution of **a** the relative error between the variances or Reynolds shear-stress predicted by the XHWA model as a function of  $\phi$  with  $h = 0$  and  $k = 0$ , and **b** the number of occurrence  $N_L$  (%) of absolute instantaneous angle  $|\Theta|$  larger than the wire angle  $\phi$  (SPIV measurements). Note the logarithmic scale of the horizontal axis in **b**. Symbols:  $\phi = 60^\circ$ , solid lines:  $\phi = 45^\circ$  and dashed lines:  $\phi = 30^\circ$



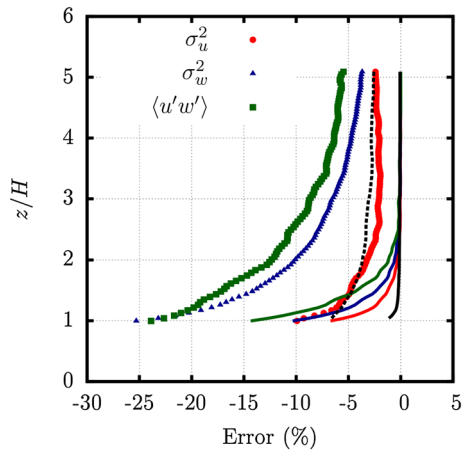


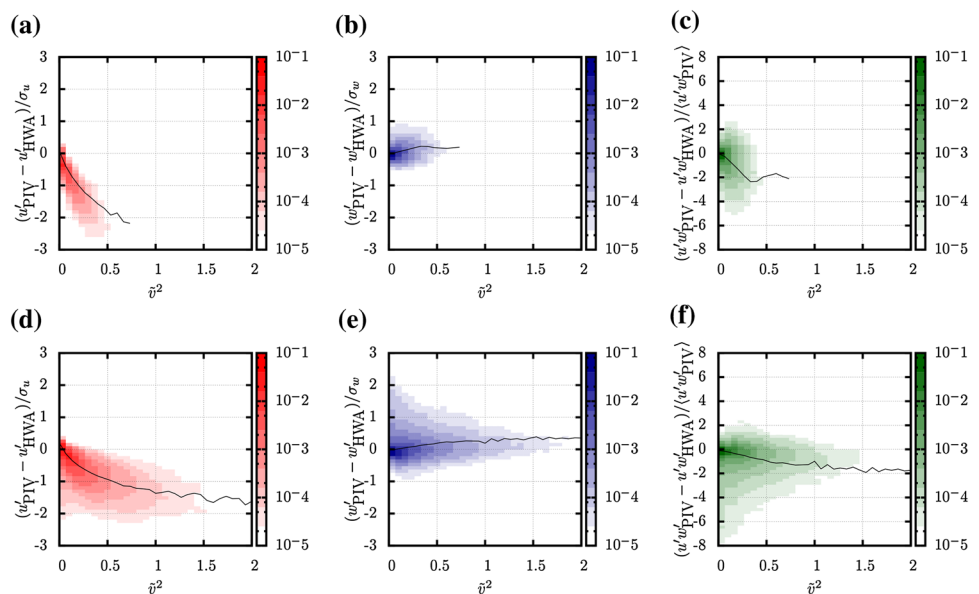
**Fig. 5** Wall-normal evolution of the relative error between the variances or Reynolds shear-stress as measured by the XHWA model and SPIV with  $h = 1.05$  (symbols),  $h = 0$  (solid lines) (with  $\phi = 45^\circ$  and  $k = 0$ ). Relative error of  $\sigma_u^2$  obtained for a single-wire HWA probe simulated with (black dashed line)  $h = 1.05$  and (solid black line)  $h = 0$  are shown for comparison

with the observed bias of XHWA measurements in flow over rough wall reported in the literature (Djenidi et al. 2014). However, the cause of this underestimation has been attributed in the past to the occurrence of strong penetration and ejection events in the roughness sublayer causing rectification, whereas, as shown here, the use of three-component PIV measurements highlights the major influence of the lateral velocity component. For comparison, a single-wire probe has been modeled as well, using only the first equation in Eq. (1), in a configuration in which the wire is along  $y$  (i.e. horizontal, parallel with  $v$ ). The relative error for  $\sigma_u^2$  (solid and dashed black lines in Fig. 5) primarily results

from the influence of the lateral velocity component and is close in magnitude to that of the XHWA probe (below 3% when  $z/H > 2$ ). Thus, the XHWA offers no advantage over the single-wire probe when only information about the streamwise velocity component is of interest.

To confirm the influence of the lateral velocity component and its impact on the XHWA measurement accuracy, joint probability density functions (jpdf) between  $\tilde{v}^2 = v_{PIV}^2 / (u_{PIV}^2 + w_{PIV}^2)$  and the difference between the instantaneous values of either  $u'$ ,  $w'$  or the shear-stress  $u'w'$  obtained via SPIV and simulated XHWA have been computed for  $h = 1.05$ . Results for  $h = 0$  (not shown here) were checked and confirmed the decorrelation of the error with  $v$ . The quantity  $\tilde{v}^2$  is used to highlight the relative importance in the cooling process of the non-measured velocity component compared to the velocity components of interest. Results obtained at  $z/H = 1.2$  and 3 (i.e. in and above the roughness sublayer, respectively) are presented in Fig. 6. When the non-measured velocity  $v$  is taken into account, the instantaneous difference between the original SPIV signals and the simulated XHWA ones becomes non-negligible with a negative correlation between the velocity difference for the  $(u'_{PIV} - u'_{HWA})$  component and  $\tilde{v}^2$  (Fig. 6d), the impact on  $w'$  is not as marked with a bias toward both negative and positive velocity difference but results in a slightly positive correlation between the  $(w'_{PIV} - w'_{HWA})$  difference and  $\tilde{v}^2$  (Fig. 6e). It must be noted here that one cannot directly relate the information provided by the jpdfs (as in Fig. 6) to the variance difference (as in Fig. 5) but one would have to evaluate the jpdfs of the quantity  $(u'_{PIV} - u'_{HWA})(u'_{PIV} + u'_{HWA})$  against  $\tilde{v}^2$ . The instantaneous shear-stress is, therefore, also impacted by the lateral component leading to an underestimation of the shear-stress by the XHWA probe the shear-stress being

**Fig. 6** Joint probability density functions between the normalized lateral velocity component  $\tilde{v}^2 = v_{PIV}^2 / (u_{PIV}^2 + w_{PIV}^2)$  and the difference between the SPIV and the XHWA model velocity fluctuations **a, d**  $u'$ , **b, e**  $w'$  and **c, f** shear-stress  $u'w'$ , computed at (top row)  $z/H = 3$  and (bottom row)  $z/H = 1.2$  with  $h = 1.05$ ,  $\phi = 45^\circ$  and  $k = 0$ . Note the logarithmic scale of the color contours. The solid black line shows the normalized averaged difference as a function of  $\tilde{v}^2$





negative (the jpdf of  $(u'w'_{PIV} - u'w'_{HWA})$  gives directly the difference of the mean shear-stresses) (Fig. 6f). Results obtained at  $z/H = 3$  where rectification influence is quasi non-existent for the  $\phi = 45^\circ$  probe show similar trend, with a narrower spread of velocity difference (Fig. 6, top row). It confirms that the presence of the non-measured velocity component, intrinsic to turbulent flows, has a direct influence on the accuracy of XHWA measurements.

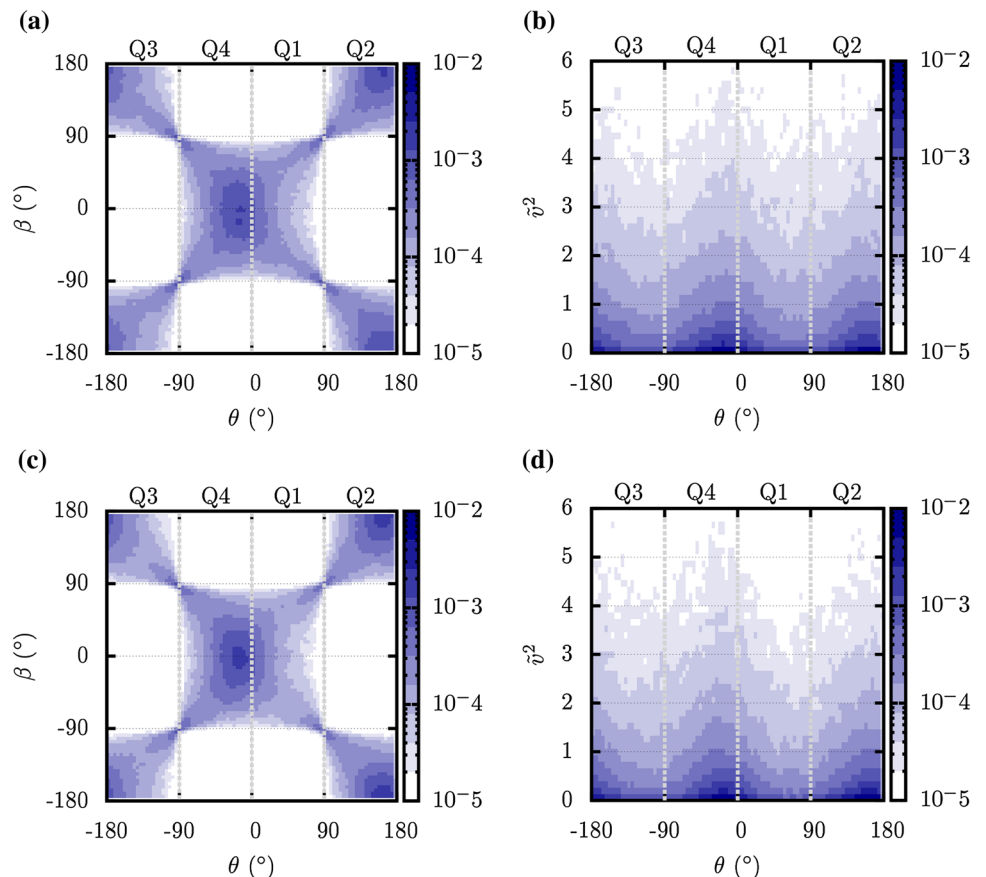
### 3.3 Link with ejection and sweep events

As mentioned in the introduction, Djenidi et al. (2014) recently confirmed that the acceptance cone angle of the XHWA probe can limit the ability of the probe to capture strong and frequent flow ejections, leading to a non-negligible bias of the quantities measured by such a probe. They also pointed out that this argument was only a partial explanation of the observed Reynolds shear-stress bias. In this section, the relationships between the XHWA error and the sweeps (forward downward Q4 motion) and ejections (backward upward Q2 motion) in the flow is investigated through a quadrant analysis based on the instantaneous angle  $\theta$  between the fluctuating velocity components  $u'$  and  $w'$ . The use of  $\theta$  allows for the partitioning of the

flow into Q1 ( $0^\circ < \theta < 90^\circ$ ) Q2 ( $90^\circ < \theta < 180^\circ$ ) Q3 ( $-180^\circ < \theta < -90^\circ$ ), and Q4 ( $-90^\circ < \theta < 0^\circ$ ) events.

Having demonstrated the importance of the non-measured velocity component  $v$  in the XHWA error, the link between Q-events and the lateral instantaneous angle  $\beta$  between the fluctuating velocity components  $u'$  and  $v'$  is first addressed. Figure 7a, c shows the jpdfs of  $\beta$  and  $\theta$  at two heights  $z/H = 1.2$  and  $3$ , respectively. In agreement with the fact that the present measurements have been performed in the symmetry plane of the cube, the calculated jpdfs are symmetric relative to  $\beta = 0$ , confirming that there is no preferential lateral inclination of the Q-events. That is also consistent with the expected statistical spanwise homogeneity of the flow above the roughness sublayer ( $z/H > 2$ ). It must be noted here that the absence of any bias in the present PIV measurements has been checked, the values of the mean spanwise velocity and the cross-correlation between  $v'$  and  $u'$  or  $w'$  being found to be zero (not shown here). Q2 and Q4 events appear to be more frequent than Q1 and Q3. However, independently of their nature, a substantial number of Q-events are laterally inclined, i.e. they are accompanied with a non-zero lateral  $v$  components. It must be noted here that the apparent significant correlation between  $\beta$  and  $\theta$  is likely due to the definition of both angles based on the inverse of  $u'$  ( $\tan \theta = w'/u'$  and  $\tan \beta = v'/u'$ ): when

**Fig. 7** Joint probability density functions between **a, c** instantaneous flow angles  $\theta$  and  $\beta$  and **b, d** between  $\theta$  and the normalized lateral velocity component  $\tilde{v}^2$ , computed at (top row)  $z/H = 3$  and (bottom row)  $z/H = 1.2$  with  $h = 1.05$ ,  $\phi = 45^\circ$  and  $k = 0$ . Note the logarithmic scale of the color contours



$u'$  goes to zero, both  $|\beta|$  and  $|\theta|$  increases towards  $90^\circ$ , for all Q-events. The quantity  $\tilde{v}^2 = v_{PIV}^2 / (u_{PIV}^2 + w_{PIV}^2)$ , identified in the present study as a diagnostic quantity to measure the error in the velocity components measured by the XHWA, shows a dependence on the nature of the considered Q-events (Fig. 7b, d). The largest bias  $\tilde{v}^2$  occurs for ejections (Q2) and sweeps (Q4), independently of the considered wall-normal location. As these events are known to be the largest contributors to the Reynolds shear-stress  $\langle u'w' \rangle$  in rough wall flows, this will lead to a poorer estimation of this key quantity.

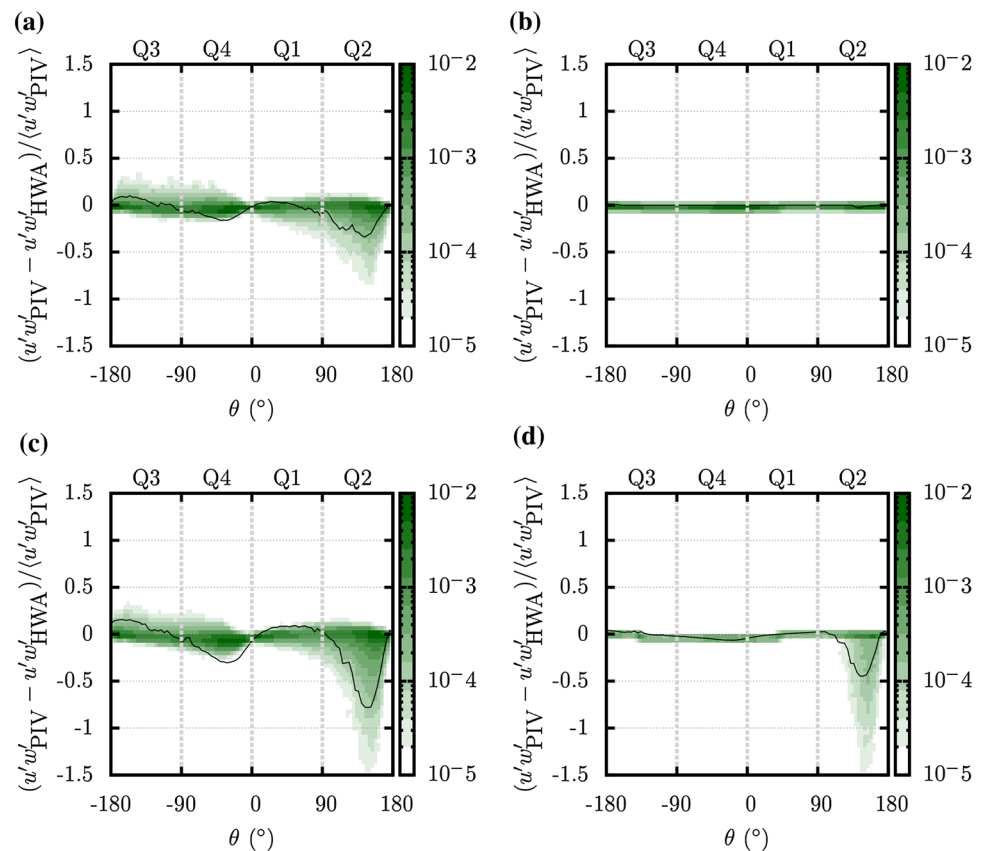
To further investigate this point, jpdfs of  $\theta$  and the normalized difference of the instantaneous shear-stress  $u'w'$  measured by PIV and XHWA are presented in Fig. 8. Both cases with ( $h = 1.05$ ) and without ( $h = 0$ ) the influence of the lateral component are shown to emphasize the role of  $v$  in the performance of XHWA probes. In the case  $h = 0$ , the only source of error is the rectification, which depends primarily on the wire-angle  $\phi$  of the probe and the dynamics of the flow (Fig. 4a). To help in the interpretation of these jpdfs and highlight the difference between Q-events, the normalized averaged difference as a function of  $\theta$  is also shown superimposed. It must be noted here that in the case of the shear-stress difference, averaging these jpdfs over the values of both variables directly gives the error shown in Fig. 5. The following conclusions are qualitatively the same

at the two investigated wall-normal locations ( $z/H = 1.2$  and  $3$ ). Results demonstrate the dependence of the instantaneous shear-stress difference on the nature of the Q-events identified via the instantaneous flow angle  $\theta$ . When the influence of  $v'$  is taken into account, all Q-events are marked by a significant number of occurrence of large shear-stress difference, Q2-events being the most affected (Fig. 8a, c). When only rectification is considered (Fig. 8b, d), the bias in  $u'w'$  measured by the XHWA probe falls to zero, except in the lowest region of the flow and concerns mostly ejections events (Q2) in agreement with Fig. 4 and with the conclusion of Djenidi et al. (2014). Comparison of Fig. 8a, c with Fig. 8b, d demonstrates that the limiting acceptance cone angle is not the sole cause for the bias in XHWA measurements. It even turns out to be a minor contributor in terms of frequency of occurrence and magnitude compared to the influence of the non-measured component  $v$  that accompanies any Q-event.

## 4 Conclusion

The performance of the measurement of the streamwise and wall-normal velocity components  $u$  and  $w$  via an XHWA probe in the lower part of a high-Reynolds number boundary layer developing over a cube array has been investigated.

**Fig. 8** Joint probability density functions between the instantaneous flow angle  $\theta$  and the normalized difference between the SPIV and the XHWA model shear-stress  $u'w'$  taking into account (a, c) or not (b, d) the influence of the lateral component, computed at (top row)  $z/H = 3$  and (bottom row)  $z/H = 1.2$  with  $\phi = 45^\circ$  and  $k = 0$ . Note the logarithmic scale of the color contours. The solid black line shows the normalized averaged difference as a function of  $\theta$



The present approach relies on SPIV measurements used to model a virtual XHWA probe using the effective cooling velocity concept in which the three velocity components of the flow can be taken into account to estimate the two velocity components in the wire plane, as measured by the XHWA probe. Influence of both the wire angle and the presence of the non-measured lateral velocity component  $v$  has been studied separately. As reported in the literature, strong instantaneous flow angles (that can be related to the occurrence to ejection and penetration events) overranging the acceptance cone angle of the probe cause rectification of the XHWA signal and lead to an underestimation of the variances of  $u$  and  $w$  and Reynolds shear-stress  $\langle u'w' \rangle$ . In the absence of lateral velocity, for a probe with a wire angle  $\phi = 45^\circ$ , this effect has been found to be confined in the roughness sublayer, for  $z/H < 2$ . Taking into account, the lateral velocity  $v$  in the probe model showed that the non-measured velocity component is a major source of error leading to a consistent underestimation of the flow statistics, with the strongest impact on the variance of the wall-normal velocity component and the Reynolds shear-stress. Given the intrinsic three-dimensional character of turbulent flows, XHWA measurements are doomed to be affected by the error caused by the non-measured velocity component  $v$ , leading to a systematic underestimation of crucial statistics such as the Reynolds shear-stress  $\langle u'w' \rangle$ . It will become negligible only when  $\tilde{v}^2 = v_{PIV}^2 / (u_{PIV}^2 + w_{PIV}^2)$  is small. It must be noted that large values of  $\tilde{v}^2$  are not necessarily associated to strong ejection and penetration events. Therefore, when performing shear-stress measurements via XHWA, the magnitude of the turbulent intensity of the often overlooked lateral velocity component should be at least estimated to assess the importance of the possible bias toward smaller values in the Reynolds shear-stress. Whenever possible, triple hot-wire probes, PIV or LDV, should be employed, bearing in mind that they present their own difficulties and sources of error,

Finally, recent wind tunnel investigation performed via SPIV in atmospheric boundary layer flows over a vegetation canopy model (Perret and Ruiz 2013) and over bidimensional roughness elements (Blackman et al. 2018) have demonstrated that the spanwise velocity component shows high level of fluctuations, comparable to that of the two other components  $u$  and  $w$ . The present conclusions regarding the performance of the XHWA in rough wall flows can, therefore, be expected to apply in these type of flows as well. It also emphasizes the need to systematically measure the three velocity components to allow for the assessment of the possible bias existing in XHWA measurements.

## References

- Antonia RA, Djenidi L (2010) On the outer layer controversy for a turbulent boundary layer over a rough wall. In: Nickels TB (ed) IUTAM symposium on the physics of wall-bounded turbulent flows on rough walls. Springer, Dordrecht, pp 77–86
- Basley J, Perret L, Mathis R (2018) Spatial modulations of kinetic energy in the roughness sublayer. *J Fluid Mech* 850:584–610
- Blackman K, Perret L, Calmet I, Rivet C (2017) Turbulent kinetic energy budget in the boundary layer developing over an urban-like rough wall using PIV. *Phys Fluids* 29(085):113
- Blackman K, Perret L, Savory E (2018) Effect of upstream flow regime and canyon aspect ratio on non-linear interactions between a street canyon flow and the overlying boundary layer. *Bound Layer Meteorol*. <https://doi.org/10.1007/s10546-018-0378-y>
- Bruun HH (1995) Hot-wire anemometry, principles and signal analysis. Oxford Science Publications, Oxford
- Castro IP, Cheng H, Reynolds R (2006) Turbulence over urban-type roughness: deductions from wind-tunnel measurements. *Bound Layer Meteorol* 118:109–131
- Cheng H, Castro IP (2002) Near wall flow over urban like roughness. *Bound Layer Meteorol* 104:229–259
- Coccal O, Dobre A, Thomas TG, Belcher SE (2007) Structure of turbulent flow over regular arrays of cubical roughness. *J Fluid Mech* 589:375–409
- Djenidi L, Antonia RA, Amielh M, Anselmet F (2014) Use of PIV to highlight possible errors in hot-wire Reynolds stress data over a 2D rough wall. *Exp Fluids* 55(10):1830
- Herpin S, Perret L, Mathis R, Tanguy C, Lasserre J (2018) Investigation of the flow inside an urban canopy immersed into an atmospheric boundary layer using laser doppler anemometry. *Exp Fluids* 59(5):80
- Müller UR (1992) Comparison of turbulence measurements with single, X and triple hot-wire probes. *Exp Fluids* 13(2):208–216
- Perret L, Ruiz T (2013) Spiv analysis of coherent structures in a vegetation canopy model flow. In: Venditti JG, Best J, Church M, Hardy RJ (eds) Coherent flow structures at Earth's surface, chapter 11. Wiley-Blackwell, New York, pp 161–174
- Perret L, Basley J, Mathis R, Piquet T (2018) Atmospheric boundary layers over urban-like terrains: influence of the plan density on the roughness sublayer dynamics. *Bound Layer Meteorol* (**Accepted**)
- Perret L, Piquet T, Basley J, Mathis R (2017) Effects of plan area densities of cubical roughness elements on turbulent boundary layers. In: Congrès Français de Mécanique, pp 1–12. <https://cfm2017.sciencesconf.org/130816>. Accessed 28 Aug 2017
- Reynolds RT, Castro IP (2008) Measurements in an urban-type boundary layer. *Exp Fluids* 45:141–156
- Rivet C (2014) Etude en soufflerie atmosphérique des interactions entre canopée urbaine et basse atmosphère par PIV stéréoscopique. Ph.D. thesis, Ecole Centrale de Nantes
- Tagawa M, Tsuji T, Nagano Y (1992) Evaluation of X-probe response to wire separation for wall turbulence measurements. *Exp Fluids* 12(6):413–421
- Tutu NK, Chevray R (1975) Cross-wire anemometry in high intensity turbulence. *J Fluid Mech* 71(4):785–800

**Publisher's Note** Springer Nature remains neutral with regard to jurisdictional claims in published maps and institutional affiliations.

## Affiliations

Laurent Perret<sup>1</sup> · Cédric Rivet<sup>1</sup>

✉ Laurent Perret  
laurent.perret@ec-nantes.fr

<sup>1</sup> LHEEA, UMR CNRS 6598, Centrale Nantes, B.P. 92101,  
44321 Nantes Cedex 3, France